Occam's razor on surfaces: renormalization of microscopic processes

2008 J. Phys.: Condens. Matter 20 304203

(http://iopscience.iop.org/0953-8984/20/30/304203)

IOP Publishing Journal of Physics: Condensed Matter

J. Phys.: Condens. Matter **20** (2008) 304203 (10pp) doi:10.1088/0953-8984/20/30/304203

Occam's razor on surfaces: renormalization of microscopic processes

Christoph A Haselwandter[1], Laurent Raymond[2], Alberto Verga[2] and Dimitri D Vvedensky[3]

[1] Department of Physics, Massachusetts Institute of Technology, Cambridge, MA 02139, USA

[2] Aix-Marseille Université, IM2NP, rue F. Joliot–Curie, BP 146, 13384 Marseille, France

[3] The Blackett Laboratory, Imperial College, London SW7 2BZ, UK

Received 8 February 2008, in final form 25 March 2008

Published 8 July 2008

Online at stacks.iop.org/JPhysCM/20/304203

Abstract

We describe a methodology for the expression of atomistic models of fluctuating interfaces as continuum equations. We begin with formally exact Langevin equations based on the atomistic transition rules, which are regularized to produce stochastic partial differential equations. Subsequent coarse graining is accomplished by calculating renormalization-group (RG) trajectories from initial conditions determined by the regularized equations. The RG analysis shows that the morphological manifestation of a given atomistic relaxation mechanism can depend on the length scales and timescales considered as well as on the dimensionality of the fluctuating interface. Even complex surface processes, after a moderate degree of coarse graining, are reduced to low-order stochastic partial differential equations. We illustrate these ideas with a model of a growing surface under the competition between the deposition of new material and the subsequent relaxation through surface diffusion. We conclude with an augmentation of our differential equations with a pinning term to account for lattice effects in the early stages of growth, where surface electron diffraction oscillations indicate layer-by-layer growth. The calculation of submonolayer morphology, which is composed of separated monolayer islands, provides an illustration of the efficacy of our method.

(Some figures in this article are in colour only in the electronic version)

1. Introduction

Many surface phenomena are macroscopic in that they are manifested over length scales from microns to meters and timescales from seconds to minutes. Prominent examples [1, 2] that have fundamental interest and substantial technological importance include corrosion, tribology, catalysis, fracture, epitaxial growth, and biological implants [3]. From a modern perspective, however, the underlying mechanisms of such phenomena are due to basic atomistic processes such as impingement, chemical reactions, and surface diffusion. The processes may be complex, and specific atomistic models may not always be available, but the fundamental principles are known.

Theoretical descriptions for the physical, structural, and chemical changes of materials caused by various types of external driving reflect this dichotomy between the microscopic and macroscopic points of view. The traditional approach, which is the basis for most engineering calculations, begins by replacing the atomic structure of matter by a continuous mass density, with corresponding replacements for other physical quantities. Differential equations are then formulated from basic physical principles, such as the conservation of energy, mass, and momentum. Continuum elasticity [4] and fluid mechanics [5] are the best known theories developed on this basis. At the opposite conceptual extreme, the increasing power and accessibility of computers over the past few decades, together with substantial algorithmic developments, has seen the emergence of *ab initio* techniques and molecular dynamics as practical large-scale simulation methodologies [6].

As an illustration of these approaches, we consider atomic diffusion. The simplest description of diffusion is a random walk on a Cartesian lattice, whose coarse-grained limit for the concentration c of mobile species is the diffusion equation,

$$\frac{\partial c}{\partial t} = D\nabla^2 c, \tag{1}$$

in which the diffusion constant $D = a_\parallel{}^2/\tau$, $a_\parallel$ is the jump length (typically the lattice constant), and τ the average jump frequency. This equation describes, for example, the introduction of controlled amounts of dopants into semiconductors, with vacancy diffusion being the transport mechanism [7]. However, improved fabrication techniques have reduced component size to the point where the diffusion constant depends on the concentration of the mobile species, so there are deviations from Fickian behavior [8], and an alternative continuum formulation is required.

There is even a richer range of diffusion mechanisms on surfaces, including, in addition to simple hopping, exchange with substrate atoms, long jumps, and sub-surface mobility [9]. Although these mechanisms may be amenable to a description in terms of a diffusion-type equation at a suitably coarse-grained scale, this masks their atomistic variety. We thereby arrive at a hierarchical view of surface diffusion, ranging from the atomic-scale resolution of *ab initio* molecular dynamics, where the Schrödinger equation is solved at each time step, to a coarse-grained description in terms of a diffusion equation whose atomistic ancestry resides in the parametrization of the diffusion constant. The challenge for modern materials physics is to seamlessly combine the atomistic and continuum descriptions into a single adaptive simulation [10, 11].

The scenario just described is an example of the simplest multiscale scheme, based on an unambiguous separation of timescales. More challenging are cases where there is an intrinsic coupling of many length scales. Turbulence is a widely cited example of an inherently multiscale phenomenon, in which there is an energy cascade from the microscopic to the macroscopic modes. In the arena of materials science, fracture also exhibits a form of energy cascade. When the stress exceeds a critical value, atomic bonds begin to break, elastic energy is released, and a new surface is created as the crack propagates in the material. For brittle fracture, atomic bonds break and the lattice appears to 'unzip' behind an atomically sharp crack tip. In the case of ductile fracture, crack propagation is accompanied by the creation of voids or the emission of dislocations and other lattice defects. The crack tip becomes blunt, reducing the stress concentration, and continued crack propagation generally requires a large input of energy. Continuous phase transitions provide another canonical example of multiscale physics, with the divergent correlation length at the critical point signaling the absence of a characteristic length.

A computational framework for each of the foregoing scenarios is provided by the renormalization group [12, 13], and the extension of these ideas to driven fluctuating interfaces is the main subject of this paper. We will concentrate on the fluctuations during epitaxial growth, where a new crystalline surface is formed as the result of deposition of new material onto a crystalline substrate, but there are many other notable examples that have attracted attention from the statistical mechanics community. These include ion sputtering of surfaces [14, 15], fracture surfaces [16, 17], burning paper [18], sandpile models of self-organized criticality [19], penetrating flux fronts in thin films of high-T_c superconductors [20], and the growth of malignant tumors [21, 22]. Although a systematic procedure for incorporating atomic degrees of freedom into coarse-grained differential equations has yet to be advanced, significant progress can been made if the atoms are confined to sites on a lattice. Atomic motion is then replaced by transitions between neighboring sites, resulting in a 'lattice gas'. Non-equilibrium phenomena in many settings are modeled by lattice gases with transition rules designed to capture the essence of atomic-scale interactions [23, 24]. Lattice gases are essentially a mesoscopic description of processes, such as diffusion, that provides the basis for a continuum formulation through a coarse graining and renormalization procedure. In this sense, our approach reduces complex surface processes to their essential continuum expressions.

The outline of this paper is as follows. In section 2, we describe our basic methodology for regularizing the master equation associated with any lattice model. This yields a low-order stochastic partial differential equation that serves as an initial condition for a subsequent renormalization-group (RG) analysis, which is illustrated in section 3 for a model of a fluctuating surface during epitaxial growth. In section 4 we describe an extension of the continuum equation derived in section 3 to include lattice effects in the early stages of growth, including island statistics prior to any significant coalescence, and the periodic filling of complete atomic layers. A summary and outlook are provided in section 5.

2. Stochastic differential equations for lattice models

2.1. The master equation

To simplify the notation and the appearance of equations, we will describe our method for a one-dimensional system. All of the following formalism has a straightforward extension to higher dimensions. We consider lattice models that are completely characterized by an array $\mathbf{H}$ of integer heights H_i at each site i of an L-site lattice $\mathbf{H} \equiv \{H_1, H_2, \ldots, H_L\}$ at each discrete time step t. The transition rates depend only on the instantaneous height profile, rather than its history, a property referred to as 'Markovian'. The evolution of Markovian lattice models is governed by the Chapman–Kolmogorov equation [25] for the transition probability $T_{t+t'}(\mathbf{H}_3|\mathbf{H}_1)$ from height configuration $\mathbf{H}_1$ to configuration $\mathbf{H}_3$ over the time interval $t + t'$,

$$T_{t+t'}(\mathbf{H}_3|\mathbf{H}_1) = \sum_{\mathbf{H}_2} T_{t'}(\mathbf{H}_3|\mathbf{H}_2)\, T_t(\mathbf{H}_2|\mathbf{H}_1), \qquad (2)$$

where $t = t_2 - t_1$ and $t' = t_3 - t_2$. The differential form of this equation, expressed in terms of the small time limit of the transition probability, is the master equation [25],

$$\frac{\partial P}{\partial t} = \sum_{\mathbf{r}} [W(\mathbf{H}-\mathbf{r};\mathbf{r})P(\mathbf{H}-\mathbf{r},t) - W(\mathbf{H};\mathbf{r})P(\mathbf{H},t)], \quad (3)$$

where $P(\mathbf{H}, t) \equiv T_t(\mathbf{H}|\mathbf{H}_1)$, $W(\mathbf{H};\mathbf{r})$ is the transition rate from $\mathbf{H}$ to $\mathbf{H} + \mathbf{r}$, and $\mathbf{r} = \{r_1, r_2, \ldots, r_L\}$ is the array of jump lengths between height configurations.

The Chapman–Kolmogorov equation (2) is the definitive statement of the evolution of Markovian systems and is solved

implicitly when performing computer simulations, which for the models that we consider are kinetic Monte Carlo (KMC) simulations. The master equation (3) is a formal restatement of the Chapman–Kolmogorov equation in the limit of continuous time, but with discrete height variables. Although the master equation is more manageable than the Chapman–Kolmogorov equation, direct solutions are available only for a few special cases. We have developed a computational framework based on the Kramers–Moyal–van Kampen expansion [25–29] and implementations of limit theorems due to Kurtz [30–37] that yield a Fokker–Planck equation, and therefrom a Langevin equation, that embodies the statistical properties of the master equation.

2.2. Lattice Langevin equations

The Kramers–Moyal–van Kampen expansion relies [25] on the expansion of the first term on the right-hand side of equation (3) in terms of the jump length $\mathbf{r}$. For this purpose we identify the 'largeness' parameter Ω governing intrinsic fluctuations [25] as the reciprocal of the particle size or deposition unit [27]. Transforming to the continuous height and time variables $h_i' = \Omega^{-1} H_i$ and $\tau' = \Omega^{-1} t$, we obtain the master equation,

$$\frac{\partial P}{\partial \tau'} = \int \Big[\widetilde{W}\left(\mathbf{h}' - \mathbf{r}; \mathbf{r}\right) P\left(\mathbf{h}' - \mathbf{r}, \tau'\right) - \widetilde{W}\left(\mathbf{h}'; \mathbf{r}\right) P\left(\mathbf{h}', \tau'\right) \Big] \mathrm{d}\mathbf{r}, \tag{4}$$

where the $\widetilde{W}$ are transition rate densities for jumps rescaled by Ω relative to the original lattice model which satisfy the smoothness and small-jump conditions required for subsequent expansions [25, 27].

The master equation (4), which is formulated in terms of continuous time and height variables, can be transformed [27–37] into the more analytically tractable lattice Langevin equation,

$$\frac{\mathrm{d}h_i}{\mathrm{d}\tau} = K_i^{(1)} + \eta_i, \tag{5}$$

for $i = 1, 2, \ldots, L$, where we have restored the original scale of the height and time variables through $h_i' \to h_i = \Omega h_i'$ and $\tau' \to \tau = \Omega \tau'$, $K_i^{(1)}$ is the first moment of the transition rate density, and the η_i are Gaussian noises that have zero mean and covariances

$$\langle \eta_i(\tau_1) \eta_j(\tau_2) \rangle = K_{ij}^{(2)} \delta(\tau_1 - \tau_2), \tag{6}$$

in which $K_{ij}^{(2)}$ is the second moment of the transition rate density. The transition moments are defined by

$$K_i^{(1)}(\mathbf{h}) = \int r_i W\left(\mathbf{h}; \mathbf{r}\right) \mathrm{d}\mathbf{r}, \tag{7}$$

$$K_{ij}^{(2)}(\mathbf{h}) = \int r_i r_j W\left(\mathbf{h}; \mathbf{r}\right) \mathrm{d}\mathbf{r}, \tag{8}$$

where W is the rescaled representation of $\widetilde{W}$ appropriate for h_i and τ.

The Kramers–Moyal–van Kampen expansion of lattice models [25, 27–29] has been used with great success in the description of fluctuations in physical systems [25]. Although this approach has several limitations [34, 35], they can be overcome [34–37] by employing limit theorems due to Kurtz [30–33]. The emphasis in these studies is on the transition from the discrete jumps of size Ω^{-1} in $\mathbf{h}'$ to corresponding 'continuous jumps' in the limit that $\Omega \to \infty$. This allows the 'control of discreteness' [34] in the system and, thus, provides a natural method for the passage from discrete to continuous variables. Accordingly, beginning with equation (4) and invoking the Kurtz theorems, one arrives [34–37] at equation (5) as $\Omega \to \infty$ under rather mild mathematical assumptions [34]. In contrast to the Kramers–Moyal–van Kampen expansion, no assumptions are made regarding the existence of an underlying deterministic description nor the size of the fluctuations [34, 36, 37].

2.3. Regularized Langevin equations

The *continuum* Langevin equation associated with the lattice Langevin equation (5) is obtained by first introducing the continuous space variable x and the analytic height function $u(x, \tau)$ that has the Taylor expansion

$$h(i \pm n, \tau) = \sum_{k=0}^{\infty} \left. \frac{\partial^k u}{\partial x^k} \right|_i \frac{(\pm a_\parallel n)^k}{k!}, \tag{9}$$

where $a_\parallel$ is the lateral lattice spacing. According to this expansion, all height variables that determine the first and second moments at site i and, hence, the lattice Langevin equation (5) at this lattice site, are represented by u and its derivatives evaluated there. For many lattice models, however, height variables appear only as arguments of non-analytic functions, such as the step function,

$$\theta_{\mathrm{d}}(\Delta h) = \begin{cases} 1, & \text{if } \Delta h \geqslant 0; \\ 0, & \text{if } \Delta h < 0, \end{cases} \tag{10}$$

where Δh is the difference between the (discrete) heights differences at nearest-neighbor sites. For example, the number of nearest neighbors n_i at site i on a one-dimensional lattice is

$$n_i = \theta_{\mathrm{d}}(h_{i-1} - h_i) + \theta_{\mathrm{d}}(h_{i+1} - h_i). \tag{11}$$

The appearance of such non-analytic functions within lattice Langevin equations requires a continuation for non-integer values of the height function [27], but presents no problems of principle. However, the regularization of these equations necessitates the representation of the non-analytic functions as limits of *analytic* functions. The regularized lattice Langevin equation is then obtained by replacing non-analytic functions by their analytic approximations, whereupon Taylor expansions are carried out to obtain a stochastic partial differential equation. The more faithful the representation that the analytic function provides of the original function, the greater the number of derivatives that appear in this equation, and the more closely the solutions of the differential equation follow those of the underlying lattice model [28, 29].

Although this procedure is systematic, the absence of a rigorous framework means that its validity must be assessed on a case-by-case basis [38].

In view of the foregoing, we represent θ_d for continuous arguments by

$$\theta(\Delta h;\delta)=\frac{1}{2a}\int_{-\infty}^{a_\perp^{-1}\Delta h}[\mathrm{erf}((s+a)\delta)-\mathrm{erf}(s\delta)]\,\mathrm{d}s, \quad (12)$$

where $\mathrm{erf}(x)$ is the error function, $0<a\leqslant 1$, $\delta>0$, and $a_\perp$ is the perpendicular lattice spacing. The Taylor expansion of θ around $\Delta h=0$ has an infinite radius of convergence for any finite δ. The values of the parameters a and δ depend on the model being studied and the spatial dimension. The discrete step function θ_d is required only for integer arguments, so a determines how this function is continued from 0 to 1 and, hence, how the rules of the lattice model are extended to continuous heights [27, 29]. The extent of smoothing of θ_d is determined by δ, with $\delta\to\infty$ providing an exact representation,

$$\theta(\Delta h)=\lim_{\delta\to\infty}\theta(\Delta h;\delta). \quad (13)$$

In practice, equation (12) is found to provide an excellent description of the atomistic transition rules for $\delta\gtrapprox 10$ [29], while smaller values of δ produce a smoothed representation of the lattice model. Accordingly, for finite δ, θ can be expanded around $\Delta h=0$ as

$$\theta(\Delta h;\delta)=A(\delta;a)+\frac{B(\delta;a)}{a_\perp}\Delta h+\frac{C(\delta;a)}{a_\perp^2}(\Delta h)^2+\cdots. \quad (14)$$

As noted above, the convergence of this expansion for all finite δ means that the coefficients of $(\Delta h)^n$ diminish with increasing n. For many atomistic processes, this allows the lattice Langevin equation (5) to be approximated by a finite-order stochastic differential equation.

2.4. Stochastic partial differential equations

The substitution of equations (9) and (14) into equation (5) produces, for small values of δ, the leading-order continuum equation describing the fundamental properties of a given lattice model. For lattice models of homoepitaxial growth, the processes typically included are some combination of random deposition, possibly followed by some form of rapid non-thermal relaxation, and nearest-neighbor thermally activated hopping. For such models, we find [28, 29] that the leading-order continuum Langevin equation obtained for small δ takes the form

$$\frac{\partial u}{\partial\tau}=\nu_2\nabla^2u-\nu_4\nabla^4u+\lambda_{13}\nabla(\nabla u)^3+\lambda_{22}\nabla^2(\nabla u)^2+\xi, \quad (15)$$

where the Gaussian noise $\xi(x,\tau)$ has zero mean and covariance

$$\langle\xi(x_1,\tau_1)\,\xi(x_2,\tau_2)\rangle=2\mathcal{D}\delta(x_1-x_1)\delta(\tau_1-\tau_2), \quad (16)$$

in which $\mathcal{D}=D_0-D_2\nabla^2$. In writing equation (15) we have made the transformation $u\to u+a_\perp\tau$ to eliminate the absolute average height of the surface profile, so that u describes the *fluctuations* about this average.

The general form of the Langevin equation (15) has been previously postulated on the basis of symmetry arguments [39–41] and subsumes several widely studied continuum equations of conserved surface growth as special cases: the Edwards–Wilkinson (EW) equation [42],

$$\frac{\partial u}{\partial\tau}=\nu_2\nabla^2u+\xi, \quad (17)$$

the Mullins–Herring (MH) equation [43, 44],

$$\frac{\partial u}{\partial\tau}=-\nu_4\nabla^4u+\xi, \quad (18)$$

the Villain–Lai–Das Sarma (VLDS) equation [39, 40],

$$\frac{\partial u}{\partial\tau}=-\nu_4\nabla^4u+\lambda_{22}\nabla^2(\nabla u)^2+\xi, \quad (19)$$

and the equation

$$\frac{\partial u}{\partial\tau}=-\nu_4\nabla^4u+\lambda_{13}\nabla(\nabla u)^3+\xi, \quad (20)$$

studied in [45]. In equations (17)–(20), $\nu_2>0$ and $\nu_4>0$ to ensure stability. Variations of the MH and the VLDS equations are the *conserved* MH (cMH) equation and the *conserved* VLDS (cVLDS) equation [46], for which the noise covariance,

$$\langle\xi(\mathbf{x}_1,\tau_1)\,\xi(\mathbf{x}_2,\tau_2)\rangle=-2\,D_2\,\nabla^2\,\delta^d(\mathbf{x}_1-\mathbf{x}_2)\,\delta(\tau_1-\tau_2), \quad (21)$$

corresponds to stochastic processes that conserve the particle number.

The justification of these equations for particular growth scenarios typically relies on phenomenological and scaling arguments [40, 41] to eliminate particular terms in equation (15). Our analysis [28, 29] suggests, however, that *all* terms in equation (15) generally have non-zero coefficients for homoepitaxial growth, at least at finite length scales and timescales. Scaling arguments can sometimes be used to identify the dominant terms at large length scales and timescales, but such approaches do not capture the crossover behavior between the transient regimes and can even sometimes lead to incorrect conclusions about the asymptotic behavior, especially in higher spatial dimensions [28]. Hence, the complete equation (15) must be used when making comparisons between continuum descriptions and computer simulations of lattice models or experiments, which access only transient regimes. Differences in the transition rules of lattice models of homoepitaxial growth enter through the relative magnitudes and signs of the coefficients [28, 29] in the leading-order equation (15). As will be discussed below, these coefficients can have a profound effect on the transformation of the equation under coarse graining.

3. Morphological evolution during molecular-beam epitaxy

Epitaxial growth by molecular-beam epitaxy (MBE) is initiated by the deposition of atoms or simple homoatomic molecules

onto a heated substrate. The deposited atoms may undergo an immediate short-range non-thermal mobility to dissipate the heat of condensation. Afterward, these adatoms acquire energy from the thermal vibrations of the substrate and hop from site to site with possible attachment and detachment involving other atoms, clusters, and step edges, prior to final incorporation into the growing surface.

Most simulations of epitaxial growth are based on KMC simulations of the solid-on-solid model [47]. The simplest implementation of this model, with only random deposition and activated nearest-neighbor hopping, has been used with great effect to explain many fundamental experimental observations, including surface diffraction oscillations [48–50], the distributions of island sizes in the submonolayer regime [51–53], and atomistic growth mechanisms of GaAs(001) [54–56]. In this section, we provide an analytic formulation of this model, study its behavior under renormalization, and compare with KMC simulations.

3.1. Stochastic differential equation for the deposition–diffusion model

The transition rates for random deposition and activated hopping are, respectively,

$$W_1(\mathbf{H};\mathbf{r}) = \tau_0^{-1} \sum_i \delta_{r_i,a_\perp} \prod_{k\neq i} \delta_{r_k,0}, \tag{22}$$

where $\delta_{i,j}$ is the Kronecker delta, and

$$W_2(\mathbf{H};\mathbf{r}) = \sum_{ij} w_{ij} \delta_{r_i,-a_\perp} \delta_{r_j,a_\perp} \prod_{k\neq i,j} \delta_{r_k,0}, \tag{23}$$

where the hopping rate and hopping rules are contained in the w_{ij}. For nearest-neighbor hopping with Arrhenius rates whose energy barrier E_i is calculated from the initial environment of the active atom, we have

$$w_{ij} = \tfrac{1}{2}\nu_0 \, \mathrm{e}^{-\beta E_i} \left(\delta_{i,j-1} + \delta_{i,j+1}\right), \tag{24}$$

where the attempt frequency $\nu_0 \sim 10^{12}$–10^{13} s^{-1} [1], $\beta = (k_\mathrm{B}T)^{-1}$, k_B is Boltzmann's constant, and T is the absolute temperature of the substrate. The simplest expression for E_i is the sum of a site-independent energy barrier E_S from the substrate and a contribution E_N from each of the n_i lateral nearest neighbors: $E_i = E_\mathrm{S} + n_i E_\mathrm{N}$. For specific materials systems, these barriers can be determined either by fitting to a particular experiment [49, 54] or from first-principles calculations [55]. The total transition rate $W = W_1 + W_2$.

The procedure outlined in section 2, with $\delta \lessapprox 0.01$, produces the leading-order stochastic differential equation for our basic model for MBE on a two-dimensional substrate [57]:

$$\frac{\partial u}{\partial \tau} = -|\nu_4| \, \nabla^4 u + \lambda_{22} \, \nabla^2 (\nabla u)^2 + F + \xi, \tag{25}$$

with

$$\nu_4 = -\frac{a_\parallel^4}{a_\perp^2} \frac{D_\mathrm{S}}{2d} B \, \gamma \, (1 - A\,\gamma)^{2d-1}, \tag{26}$$

$$\lambda_{22} = -\frac{a_\parallel^4}{a_\perp^3} \frac{D_\mathrm{S}}{2d} \gamma \, (1 - A\gamma)^{2d-2} \left[B^2\gamma + 2\,C\,(1 - A\gamma)\right], \tag{27}$$

in which $A \approx 0.5$, $B \approx 0.006$, and $C \approx -3 \times 10^{-7}$ for $\delta \approx 0.01$,

$$\gamma = 1 - \mathrm{e}^{-\beta E_\mathrm{N}}, \tag{28}$$

$$D_\mathrm{S} = a_\perp^2 \, \nu_0 \, \mathrm{e}^{-\beta E_\mathrm{S}}, \tag{29}$$

the deposition flux $F = a_\perp/\tau_0$, and the smoothed Gaussian noise $\xi(\mathbf{x}, \tau)$ has zero mean and covariance

$$\langle \xi(\mathbf{x}_1, t_1)\xi(\mathbf{x}_2, \tau_2)\rangle = 2\mathcal{D}\delta^d(\mathbf{x}_1 - \mathbf{x}_2)\delta(\tau_1 - \tau_2), \tag{30}$$

with $\mathcal{D} = D_0 - D_2\nabla^2$, and

$$D_0 = a_\parallel^d \frac{a_\perp^2}{2\tau_0}, \tag{31}$$

$$D_2 = a_\parallel^{d+2} \frac{D_\mathrm{S}}{2d} \, (1 - A\,\gamma)^{2d}. \tag{32}$$

Our results provide a fundamental confirmation of various phenomenological arguments [39, 40, 58] that have been used to justify the general form of equation (25) as the equation for epitaxial growth with random deposition and surface diffusion. This equation has full two-dimensional rotational symmetry, despite the original model being defined on a square lattice. This results from the fact that our description of surface diffusion depends on the local environment only of the initial site. In models where the transition rates also involve information about potential target sites (e.g. [59]), the corresponding differential equations have mixed derivatives that reflect the square symmetry of the lattice.

The magnitudes and signs of the coefficients ν_4, λ_{22}, D_0, and D_2 are determined directly by the rules of the atomistic model, the numerical values of the growth parameters (T and F), and the dimensionality of the substrate. The quantities A, B, and C that enter through the expansion in (14) depend both on the analytic representation and on the smoothing parameter δ. That their orders of magnitude follow the inequality $A \gg B \gg C$ indicates that equation (25) contains the dominant terms of the regularized description, as can indeed be confirmed by comparing the magnitudes of the coefficients in equation (25) with the magnitudes of the coefficients of higher-order terms. The combination of all of these factors allows the systematic investigation of the interplay between deposition and diffusion for any length scales and timescales, as will be shown below.

3.2. Renormalization-group analysis

The multiscale analysis of the fluctuating surface described by equation (25) is based on calculating the RG trajectories from the initial conditions in equations (26)–(32). A previous RG analysis [58] revealed that the noise covariance is modified to $\mathcal{D} = D_0 - D_2\nabla^2 + D_4\nabla^4$ under RG transformations, where we have that $D_4 = 0$ in our leading-order equation (25). A non-zero value for D_4 affects the location of the fixed points, but does not alter the values of the exponents. The coefficients in equation (25) renormalize under the scale changes $\mathbf{x} \to \mathrm{e}^{\ell}\mathbf{x}$,

$\tau \to e^{z\ell}\tau$, and $u \to e^{\alpha\ell}u$ to one-loop order according to [40, 58]

$$\frac{d\nu_4}{d\ell} = (z-4)\,\nu_4 - \frac{K_d}{d}\frac{D_s\,\lambda_{22}^2\,\Lambda^{d-4}}{\nu_4^2}, \tag{33}$$

$$\frac{d\lambda_{22}}{d\ell} = (z-4+\alpha)\lambda_{22}, \tag{34}$$

$$\frac{dD_0}{d\ell} = (z-d-2\alpha)\,D_0, \tag{35}$$

$$\frac{dD_2}{d\ell} = (z-d-2\alpha-2)\,D_2, \tag{36}$$

$$\frac{dD_4}{d\ell} = (z-d-2\alpha-4)\,D_4 + K_d\,\frac{\lambda_{22}^2 D^2\,\Lambda^{d-8}}{\nu_4^3}, \tag{37}$$

where $K_d = S_d/(2\pi)^d$, $S_d = 2\pi^{d/2}/\Gamma(\frac{1}{2}d)$ is the surface area of a d-dimensional unit sphere,

$$D_s = \sum_{i=0}^{2}(d-6+2i)D_{2i}\,\Lambda^{2i}, \tag{38}$$

$$D = D_0 + D_2\,\Lambda^2 + D_4\,\Lambda^4, \tag{39}$$

and Λ is the momentum cutoff. The smallest length scale in our lattice model is the atomic spacing, so we have $\Lambda = 2\pi\,a_\parallel^{-1}$. As for any equation combining conserved dynamics with non-conserved noise, the parameter D_0 does not renormalize to any order in perturbation theory [58], so the scaling relation $z - 2\alpha = d$ implied by equation (35) is exact.

To investigate crossover regimes, we introduce the dimensionless quantities

$$r = \frac{D_0\lambda_{22}^2}{\nu_4^3}\,\Lambda^{d-4}, \qquad \Gamma_2 = \frac{D_2}{D_0}\Lambda^2, \qquad \Gamma_4 = \frac{D_4}{D_0}\,\Lambda^4, \tag{40}$$

in terms of which the RG equations (33)–(37) do not directly depend on z and α:

$$\frac{dr}{d\ell} = (4-d)r + \frac{3\,K_d}{d}r^2\Gamma, \tag{41}$$

$$\frac{d\Gamma_2}{d\ell} = -2\,\Gamma_2, \tag{42}$$

$$\frac{d\Gamma_4}{d\ell} = -4\,\Gamma_4 + K_d r(1+\Gamma_2+\Gamma_4)^2, \tag{43}$$

with $\Gamma = d - 6 + (d-4)\,\Gamma_2 + (d-2)\,\Gamma_4$.

Equations (41)–(43) are the basis of our multiscale analysis of random deposition and activated nearest-neighbor hopping. There are several aspects of their derivation and applications that merit discussion. As equation (41) makes clear, the upper critical dimension of this theory $d_c = 4$. Thus, the loop expansion used to derive equations (33)–(37) is a perturbation expansion in $\varepsilon = 4 - d$, where d is the substrate dimension. For real epitaxial surfaces, $d = 2$, i.e. $\varepsilon = 2$, so it is not immediately apparent that our one-loop equations are appropriate for describing the morphological evolution of such systems [60]. A similar objection, but motivated by different considerations, was raised by Janssen [61], who found, however, that two-loop corrections are small enough to be unresolvable in experiments or simulations. Katzav [62] has even suggested that there are no higher loop corrections for such models. Our comparisons between RG trajectories calculated from equations (41)–(43) and KMC simulations provide additional evidence that corrections to the one-loop calculation are small and do not substantially alter the qualitative behavior of the solutions.

3.3. Fixed points

The fixed points of the RG equations (41)–(43) are straightforward to determine in the usual manner by solving the three equations $dr/d\ell = 0$, $d\Gamma_2/d\ell = 0$, and $d\Gamma_4/d\ell = 0$ with $d = 2$. There are three solutions. The MH fixed point,

$$r^* = 0, \qquad \Gamma_2^* = 0, \qquad \Gamma_4^* = 0, \tag{44}$$

is located at the origin, and there are two fixed points corresponding to the VLDS equation:

$$r^* = \frac{2\pi}{3}, \qquad \Gamma_2^* = 0, \qquad \Gamma_4^* = 5 \pm 2\sqrt{6}, \tag{45}$$

which differ only in the value of Γ_4^*. We refer to the fixed point with $\Gamma_4^* = 5 - 2\sqrt{6}$ as VLDS$^-$, and that with $\Gamma_4^* = 5 + 2\sqrt{6}$ as VLDS$^+$. Linearization around these fixed points shows that MH and VLDS$^+$ are unstable, while VLDS$^-$ is stable. Thus, the RG flow in the (r, Γ_2, Γ_4) subspace is always directed toward the VLDS$^-$ fixed point.

3.4. Renormalization-group trajectories

Figure 1(a) shows the RG trajectories for $d = 2$ with the growth conditions in [63]. The VLDS equation is approached asymptotically irrespective of the temperature, as noted above. At $T = 550$ and 575 K the initial surface morphology is dominated by the competition between the MH fixed point and random deposition, which is in agreement with the simulations in [63]. As the temperature is increased surface diffusion becomes more active and the initial conditions shift towards cMH behavior, described by equations (18) and (21). For $T \sim 600$–650 K we find that the initial surface morphology is described by the MH equation (18), but with noise covariance

$$\langle\xi(\mathbf{x}_1,\tau_1)\xi(\mathbf{x}_2,\tau_2)\rangle = 2\left(D_0 - D_2\nabla^2\right)\delta^2(\mathbf{x}_1-\mathbf{x}_2)\delta(\tau_1-\tau_2) \tag{46}$$

for the first few monolayers deposited. However, the cMH equation implies that $\beta = 0$ and standard dynamic scaling breaks down [41]. In this temperature range the initial behavior is a complex combination of fundamentally different physical mechanisms and the conventional analysis of simulation data becomes insufficient. Simulations for $T = 600$ K in [63] nevertheless show clear scaling behavior consistent with the VLDS equation even for early times. The corresponding RG trajectory in figure 1(a), on the other hand, suggests that this is merely a coincidence arising from the competing influences of MH and cMH behavior.

Figure 1(b) shows RG trajectories for the parameters in [64], also for $d = 2$. The simulations in [64] show a steeper

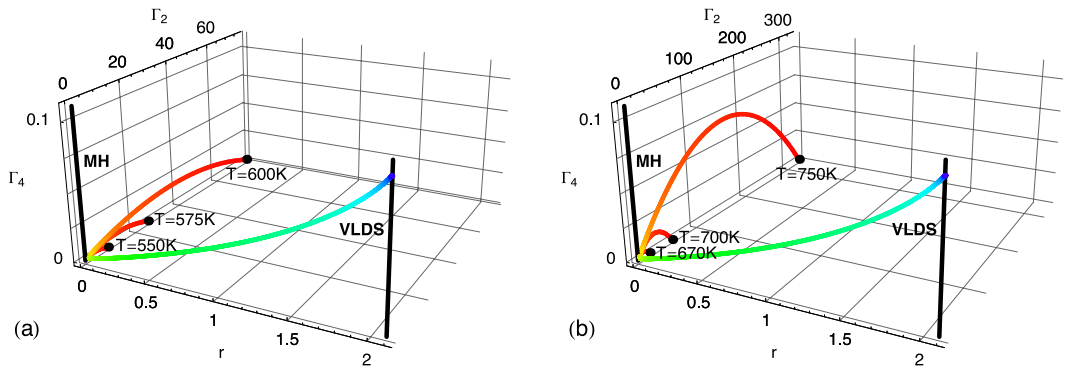

Figure 1. RG trajectories obtained from equations (41)–(43) with the initial conditions in equations (25)–(32) for $d = 2$ with $\nu_0 = 5 \times 10^{12}$ s^{-1}, $E_N = 0.24$ eV, and (a) $E_S = 1.3$ eV, $\tau_0 = 1$ s [63], and (b) $E_S = 1.58$ eV, $\tau_0 = 2$ s [64]. The black points denote initial conditions for the indicated temperatures, and the RG flow is always directed towards the VLDS fixed point.

gradient for $T = 670$ K at early times, which is at least in qualitative agreement with the initial dominance of the MH fixed point suggested by figure 1(b). For $T = 700$ K, on the other hand, simulations reveal a slightly smaller gradient in the initial transient regime [64] which, as in figure 1(a) for $T = 600$ K, suggests an incipient influence of the cMH equation for which the dynamic scaling is not valid in $d = 2$. For even higher temperatures the value for β obtained from simulations decreases further and clear scaling behavior is no longer obtained [64], consistent with the growing influence of the cMH equation on the initial dynamics predicted by figure 1(b).

The crossovers in figure 1 illustrate the inherent difficulties encountered [65–69] when attempting to describe growth morphologies observed in experiments on the basis of postulated continuum equations. Even if there is reason to expect that the morphological evolution of a system is described by the VLDS equation, our and previous [40] RG analyses show that this is only an *asymptotic* fixed point. Transient regimes, where experiments are most often carried out, are described by the MH equation.

4. Early stages of growth with a continuum equation

The lattice Langevin equation (5) provides the same level of description as KMC simulations [27], while the method used to obtain the regularized equation (25) provides a way of smoothing the discrete atomistic transition rules. In this section we investigate the extent to which equation (25) can be used in the earliest stages of growth to describe the submonolayer regime. There are several benefits of having a continuum description of submonolayer growth. The distribution of island sizes prior to any significant coalescence exhibits scaling [51–53], with the form of the scaling function providing information about the island formation kinetics. KMC simulations are capable of accounting for the experimental results [51–53], but analytic discussions of scaling have been confined to rate equations [70, 71]. Within the rate equation framework, the complete form of the scaling function requires expressions for 'capture numbers', quantities that describe the ability of an island to capture migrating adatoms. But, capture numbers are not easily accessible because they reflect the local spatial environment of an island [72]. Thus, an alternative continuum representation of submonolayer growth that is based on transition rates and implicitly incorporates the local environment of islands has distinct conceptual and computational advantages.

The regularized equation (25) describes the evolution of continuous heights as a function of continuous time and continuous lateral position. However, the morphology during submonolayer growth is composed of discrete islands with a height of a single vertical lattice spacing. Thus, this regime is characterized by non-linearities, which are responsible for nucleation and growth, and by lattice effects, which pin the island heights to increments of $a_\perp$. Accordingly, we proceed by augmenting equation (25) as follows:

$$\frac{\partial u}{\partial \tau} = -\nabla^2\left[|\nu_4|\nabla^2 u + \lambda_{22}(\nabla u)^2 - Q\sin\left(\frac{2\pi u}{a_\perp} + \frac{2\pi F\tau}{a_\perp}\right)\right] + \xi, \tag{47}$$

with

$$\langle \xi(\mathbf{x}_1, \tau_1)\xi(\mathbf{x}_2, \tau_2)\rangle = -2D_2\nabla^2\delta(\mathbf{x}_1 - \mathbf{x}_2)\delta(\tau_1 - \tau_2). \tag{48}$$

The sine term accounts for vertical lattice effects by favoring integer multiples of the vertical lattice spacing [73]. The flux term in the argument results from the usual transformation to eliminate the additive flux on the right-hand side of this equation. Note the absence of a flux contribution to the noise. This is in accord both with figure 1 when surface diffusion is active, and with previous work [74] that showed that diffusion noise dominates over deposition noise in the early stages of growth under typical growth conditions.

Figure 2 shows the surface morphology and the corresponding contour plot obtained from the numerical integration of equations (47) and (48) at 0.3 ML. The effect of the lattice pinning term is clearly seen from the fact that, despite the continuum character of the equation, there are discernible monolayer height islands. At very low coverage, the surface morphology is dominated by small noisy structures, while at higher coverages, well defined islands appear, as shown in figure 2. Additional deposition results in the periodic completion of layers followed by the nucleation of the next

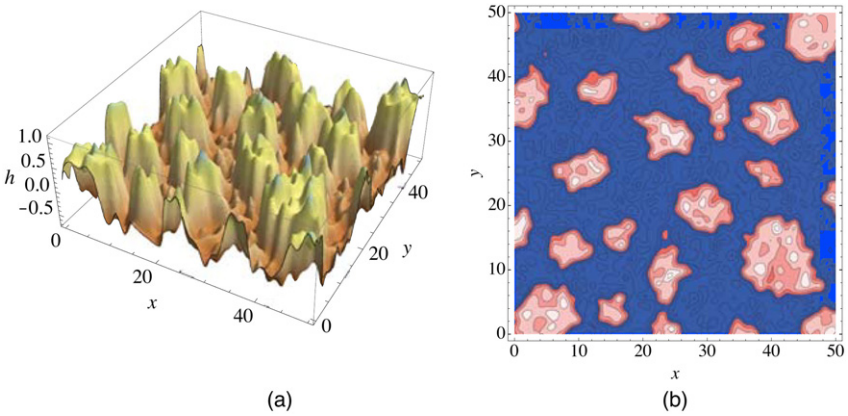

Figure 2. (a) Surface and (b) contour plots of the morphology produced from the numerical integration of equations (47) and (48) at 0.3 ML. The model parameters were $E_S = 1.5$ eV, $E_N = 0.3$ eV, and $F = 0.0.1$ ML s^{-1}, yielding $D/F \sim 10^5$. In (b), the blue contours correspond to the substrate ($h < 0$) and the red contours to the islands ($h > 0$).

layer. In fact, the next layer is initiated prior to the completion of the preceding layer, as is also observed in KMC simulations. The distribution of island sizes shows a qualitative similarity to that obtained with KMC simulation under similar growth conditions and model parameters. A detailed analysis of equations (47) and (48) will appear elsewhere, but we can already see that this model provides a basis for extending the continuum description of fluctuating interfaces to include the prevalent lattice effects in the early stages of growth.

5. Summary and discussion

We have described a procedure for transforming transition rules defined on a lattice into stochastic differential equations that describe the interface fluctuations over any given range of length scales and timescales. As the fast short-wavelength fluctuations are subsumed into an effective equation for the remaining fluctuations, the description of even complex atomistic processes reduces to a low-order stochastic partial differential equation. The machinery for carrying out this procedure is that of the renormalization group and many of the concepts familiar from applications to equilibrium phase transitions and near-equilibrium dynamics find an expression in the description of driven fluctuating interfaces. For example, the phenomenon of crossover, whereby a RG trajectory passes near one or more fixed points before proceeding to the asymptotically stable fixed point, is seen as equations that describe the transient behavior of a system that differ qualitatively from the equations that correspond to the stable fixed point.

Our methodology has been illustrated with an application to a basic model of MBE [57] that includes random deposition and surface diffusion by nearest-neighbor hopping. The system of RG equations (33)–(37), together with the initial values for the coefficients in equations (25)–(32), provide a continuum description of this model for any length scales and timescales—from the atomistic resolution of the original transition rules to the macroscopic realm. The parameters in these coarse-grained continuum equations are determined by the underlying lattice model and, hence, a direct comparison between continuum equations and growth experiments becomes feasible. In particular, our procedure can be used to predict transient surface morphologies as a function of the growth conditions, which is important for modeling device fabrication [67, 68]. Equations (5), (15), and (33)–(37) therefore establish a first-principles multiscale description our model for MBE. The results obtained using this methodology for this and other models are found to be in agreement with all available computer simulations.

Finally, we have described a way of extending our regularized models to include lattice effects in the early stages of growth. The addition of a lattice pinning term to the continuum equation produces morphologies that are in qualitative agreement with those obtained from KMC simulations. Further work will be required to more firmly establish the quantitative effectiveness of our procedure throughout the early stages of growth, but our preliminary results already suggest that even highly resolved processes such as island nucleation and growth are amenable to a continuum description.

Taken together, the results presented here and elsewhere indicate that a wide range of surface processes can be accurately described by low-order stochastic partial differential equations whose coefficients embody their atomistic characteristics. In this respect, we have applied Occam's razor to systematically express these processes in their simplest form.

Acknowledgments

This work was supported at Imperial College London by funds from the UK Engineering and Physical Sciences Research Council and the European Commission Sixth Framework Programme as part of the European Science Foundation EUROCORES Programme on Self-Organized Nanostructures (SONS). CAH is supported at MIT by an Erwin Schrödinger fellowship of the Austrian Science Fund. DDV is grateful to the University of Aix-Marseille for their hospitality during September 2007, when some of the work described here was initiated.

References

[1] Zangwill A 1988 *Physics at Surfaces* (Cambridge: Cambridge University Press)
[2] Somorjai G 1994 *Introduction to Surface Chemistry and Catalysis* (New York: Wiley Interscience)
[3] Kasemo B 2002 Biological surface science *Surf. Sci.* **500** 656–77
[4] Landau L D and Lifschitz E M 1981 *Theory of Elasticity* 2nd edn (Oxford: Pergamon)
[5] Landau L D and Lifschitz E M 1987 *Fluid Mechanics* 2nd edn (Oxford: Pergamon)
[6] Kadau K, Germann T C and Lomdahl P S 2006 Molecular dynamics comes of age: 320 billion atom simulation on BlueGene/L *Int. J. Mod. Phys.* C **17** 1755–61
[7] Brodie I and Muray J J 1982 *The Physics of Microfabrication* (New York: Plenum)
[8] Beke D L, Erdélyi Z, Langer G A, Csik A and Katona G L 2005 Diffusion on the nanometer scale *Vacuum* **80** 87–91
[9] Antczak G and Ehrlich G 2007 Jump processes in surface diffusion *Surf. Sci. Rep.* **62** 39–61
[10] Vvedensky D D 2004 Multiscale modelling of nanostructures *J. Phys.: Condens. Matter* **16** R1537–76
[11] Ala-Nissila T and Ying S C 1990 Universal properties of classical surface diffusion *Phys. Rev. Lett.* **65** 879–82
[12] Ma S-K 1976 *Modern Theory of Critical Phenomena* (Reading, MA: Benjamin/Cummings)
[13] Goldenfeld N 1992 *Lectures on Phase Transitions and the Renormalization Group* (Reading, MA: Addison-Wesley)
[14] Makeev M A and Barabási A L 1997 Ion-induced effective surface diffusion in ion sputtering *Appl. Phys. Lett.* **71** 2800–2
[15] Kim T C, Ghim C-M, Kim H J, Kim D H, Noh D Y, Kim N D, Chung J W, Yang J S, Chang Y J, Noh T W, Kahng B and Kim J-S 2004 Kinetic roughening of ion-sputtered Pd(001) surface: beyond the Kuramoto–Sivashinsky model *Phys. Rev. Lett.* **92** 246104
[16] Mandelbrot B B, Passoja D D and Paullay A J 1984 Fractal character of fracture surfaces of metals *Nature* **308** 721–2
[17] Bouchbinder E, Procaccia I, Santucci S and Vanel L 2006 Fracture surfaces as multiscaling graphs *Phys. Rev. Lett.* **96** 055509
[18] Myllys M, Maunuksela J, Alava M J, Ala-Nissila T and Timonen J 2000 Scaling and noise in slow combustion of paper *Phys. Rev. Lett.* **84** 1946–9
[19] Alava M J and Chattopadhyay A K 2004 Fluctuations and correlations in sandpiles and interfaces with boundary pinning *Phys. Rev.* E **69** 016104
[20] Surdeanu R, Wijngaarden R J, Visser E, Huijbregtse J M, Rector J H, Dam B and Griessen R 1999 Penetrating flux fronts in high-T_c thin film superconductors *Phys. Rev. Lett.* **83** 2054–7
[21] Brú A, Pastor J M, Fernaud I, Brú I, Melle S and Berenguer C 1998 Super-rough dynamics on tumor growth *Phys. Rev. Lett.* **81** 4008–11
[22] Brú A, Albertos S, Subiza J L, García-Asenjo J L and Brú I 2003 The universal dynamics of tumor growth *Biophys. J.* **85** 2948–61
[23] Rothman D H and Zaleski S 1997 *Lattice-Gas Cellular Automata: Simple Models of Complex Hydrodynamics* (Cambridge: Cambridge University Press)
[24] Chopard B and Droz M 1998 *Cellular Automata Modeling of Physical Systems* (Cambridge: Cambridge University Press)
[25] van Kampen N G 1992 *Stochastic Processes in Physics and Chemistry* 2nd edn (Amsterdam: North-Holland)
[26] Vvedensky D D, Zangwill A, Luse C N and Wilby M R 1993 Stochastic equations of motion for epitaxial growth *Phys. Rev.* E **48** 852–62
[27] Chua A L-S, Haselwandter C A, Baggio C and Vvedensky D D 2005 Langevin equations for fluctuating surfaces *Phys. Rev.* E **72** 051103(R)
[28] Haselwandter C A and Vvedensky D D 2007 Multiscale theory of fluctuating interfaces: renormalization of atomistic models *Phys. Rev. Lett.* **98** 046102
[29] Haselwandter C A and Vvedensky D D 2007 Renormalization of stochastic lattice models: basic formulation *Phys. Rev.* E **76** 041115
[30] Kurtz T G 1971 Limit theorems for sequences of jump Markov processes approximating ordinary differential processes *J. Appl. Probab.* **8** 344–56
[31] Kurtz T G 1972 The relationship between stochastic and deterministic models for chemical reactions *J. Chem. Phys.* **57** 2976–8
[32] Kurtz T G 1976 Limit theorems and diffusion approximations for density dependent Markov chains *Math. Prog. Stud.* **5** 67–78
[33] Kurtz T G 1978 Strong approximation theorems for density dependent Markov chains *Stoch. Process Appl.* **6** 223–40
[34] Horsthemke W and Brenig L 1977 Non-linear Fokker–Planck equation as an asymptotic representation of the master equation *Z. Phys.* B **27** 341–8
[35] Horsthemke W, Malek-Mansour M and Brenig L 1977 Mean-field theory of critical behaviour and first order transition: a comparison between the master equation and the nonlinear Fokker–Planck equation *Z. Phys.* B **28** 135–9
[36] Hänggi P 1978 On derivations and solutions of master equations and asymptotic representations *Z. Phys.* B **30** 85–95
[37] Fox R F and Keizer J 1991 Amplification of intrinsic fluctuations by chaotic dynamics in physical systems *Phys. Rev.* A **43** 1709–20
[38] Katzav E and Schwartz M 2004 What is the connection between ballistic deposition and the Kardar–Parisi–Zhang equation? *Phys. Rev.* E **70** 061608
[39] Villain J 1991 Continuum models of crystal growth from atomic beams with and without desorption *J. Physique* I **1** 19–42
[40] Lai Z-W and Das Sarma S 1991 Kinetic growth with surface relaxation: continuum versus atomistic models *Phys. Rev. Lett.* **66** 2348–51
[41] Barabási A-L and Stanley H E 1995 *Fractal Concepts in Surface Growth* (Cambridge: Cambridge University Press)
[42] Edwards S F and Wilkinson D R 1982 The surface statistics of a granular aggregate *Proc. R. Soc.* A **381** 17–31
[43] Herring C 1951 *The Physics of Powder Metallurgy* ed W E Kingston (New York: McGraw-Hill) pp 143–79
[44] Mullins W W 1957 Theory of thermal grooving *J. Appl. Phys.* **28** 333–9
[45] Das Sarma S and Kotlyar R 1994 Dynamical renormalization group analysis of fourth-order conserved growth nonlinearities *Phys. Rev.* E **50** R4275–8
[46] Sun T, Guo H and Grant M 1989 Dynamics of driven interfaces with a conservation law *Phys. Rev.* A **40** 6763–6
[47] Weeks J D and Gilmer G H 1979 Dynamics of crystal growth *Adv. Chem. Phys.* **40** 157–228
[48] Clarke S and Vvedensky D D 1987 Origin of reflection high-energy electron-diffraction intensity oscillations during molecular-beam epitaxy: a computational modeling approach *Phys. Rev. Lett.* **58** 2235–8
[49] Shitara T, Vvedensky D D, Wilby M R, Zhang J, Neave J H and Joyce B A 1992 Step-density variations and reflection high-energy electron-diffraction intensity oscillations during epitaxial growth on vicinal GaAs(001) *Phys. Rev.* B **46** 6815–24
[50] Šmilauer P and Vvedensky D D Step-edge barriers on GaAs(001) *Phys. Rev.* B **48** 17603–6

[51] Bartelt M C and Evans J W 1992 Scaling analysis of diffusion-mediated island growth in surface adsorption processes *Phys. Rev.* B **46** 12675–87
[52] Ratsch C, Zangwill A, Šmilauer P and Vvedensky D D 1994 Saturation and scaling of epitaxial island densities *Phys. Rev. Lett.* **72** 3194–7
[53] Amar J G and Family F 1995 Critical cluster size: island morphology and size distribution in submonolayer epitaxial growth *Phys. Rev. Lett.* **74** 2066–9
[54] Itoh M, Bell G R, Avery A R, Jones T S, Joyce B A and Vvedensky D D 1998 Island nucleation and growth on reconstructed GaAs(001) surfaces *Phys. Rev. Lett.* **81** 633–6
[55] Kratzer P and Scheffler M 2002 Reaction-limited island nucleation in molecular beam epitaxy of compound semiconductors *Phys. Rev. Lett.* **88** 036102
[56] Grosse F and Gyure M F 2002 *Ab initio* based modeling of III–V semiconductor surfaces: thermodynamic equilibrium and growth kinetics on atomic scales *Phys. Rev.* B **66** 075320
[57] Haselwandter C A and Vvedensky D D 2007 Fluctuation regimes of driven epitaxial surfaces *Europhys. Lett.* **77** 38007
[58] Tang L-H and Nattermann T 1991 Kinetic roughening in molecular-beam epitaxy *Phys. Rev. Lett.* **66** 2899–902
[59] Haselwandter C A and Vvedensky D D 2006 Stochastic equation for the morphological evolution of heteroepitaxial thin films *Phys. Rev.* B **74** 121408(R)
[60] Das Sarma S 1997 Dynamic scaling in epitaxial growth 1997 *Preprint* cond-mat/9705118v2
[61] Janssen H K 1997 On critical exponents and the renormalization of the coupling constant in growth models with surface diffusion *Phys. Rev. Lett.* **78** 1082–5
[62] Katzav E 2002 Self-consistent expansion for the molecular beam epitaxy equation *Phys. Rev.* E **65** 032103
[63] Wilby M R, Vvedensky D D and Zangwill A 1992 Scaling in a solid-on-solid model of epitaxial growth *Phys. Rev.* B **46** 12896–8
[64] Kotrla M and Šmilauer P 1996 Nonuniversality in models of epitaxial growth *Phys. Rev.* B **53** 13777–92
[65] Ballestad A, Ruck B J, Adamcyk M, Pinnington T and Tiedje T 2001 Evidence from the surface morphology for nonlinear growth of epitaxial GaAs films *Phys. Rev. Lett.* **86** 2377–80
[66] Ballestad A, Ruck B J, Schmid J H, Adamcyk M, Nodwell E, Nicoll C and Tiedje T 2002 Surface morphology of GaAs during molecular beam epitaxy growth: comparison of experimental data with simulations based on continuum growth equations *Phys. Rev.* B **65** 205302
[67] Kan H-C, Shah S, Tadyyon-Eslami T and Phaneuf R J 2004 Transient evolution of surface roughness on patterned GaAs(001) during homoepitaxial growth *Phys. Rev. Lett.* **92** 146101
[68] Kan H-C, Ankam R, Shah S, Micholsky K M, Tadyyon-Eslami T, Calhoun L and Phaneuf R J 2006 Evolution of patterned GaAs(001) during homoepitaxial growth: size versus spacing *Phys. Rev.* B **73** 195410
[69] Tadayyon-Eslami T, Kan H-C, Calhoun L C and Phaneuf R J 2006 Temperature-driven change in the unstable growth mode on patterned GaAs(001) *Phys. Rev. Lett.* **97** 126101
[70] Vvedensky D D 2000 Scaling functions for island-size distributions *Phys. Rev.* B **62** 15435–8
[71] Popescu M N, Amar J G and Family F 2001 Rate-equation approach to island size distributions and capture numbers in submonolayer irreversible growth *Phys. Rev.* B **64** 205404
[72] Mulheran P A and Blackman J A 1995 The origins of island size scaling in heterogeneous film growth *Phil. Mag. Lett.* **72** 55–60
[73] Hwa T, Kardar M and Paczuski M 1991 Growth-induced roughening of crystalline facets *Phys. Rev. Lett.* **66** 441–4
[74] Ratsch C, Gyure M F, Chen S, Kang M and Vvedensky D D 2000 Fluctuations and scaling in aggregation phenomena *Phys. Rev.* B **61** R10598–601